Photoionization of the excited $1s^2 2s2p\ ^{1,3}P^o$ states of atomic beryllium

Dae-Soung Kim
Department of Internet Business, Songho College, Heongsung Gun, Kangwon-Do 225-800, Republic of Korea

Hsaio-Ling Zhou and Steven T. Manson
Department of Physics and Astronomy, Georgia State University, Atlanta, Georgia 30303

Swaraj S. Tayal
Department of Physics, Clark Atlanta University, Atlanta, Georgia 30314
(Received 2 May 2001; published 13 September 2001)

Photoionization cross sections for ionization to $Be^+(2s,2p,3s,$ and $3p)$ states from the excited $2s2p\ ^{1,3}P^o$ states of atomic beryllium have been calculated using a noniterative eigenchannel *R*-matrix method. All associated partial photoionization cross sections are also presented. The cross sections contain a number of autoionizing Rydberg series of resonances converging to the $Be^+(2p,3s,3p,$ and $3d)$ states. Lower members of the Rydberg series of resonances with $n \leqslant 12$ are identified and resonance positions E_r, effective quantum numbers n^*, and widths Γ are presented. Excellent agreement between length and velocity gauge results is found, along with overall good agreement with previous work.

DOI: 10.1103/PhysRevA.64.042713 PACS number(s): 32.80.Fb

I. INTRODUCTION

Photoionization of the ground $2s^2\ ^1S$ state of atomic Be has been the subject of several theoretical and experimental studies in the past [1–14]. The photoionization of the excited states of Be has also been considered [6,9,10]. These studies are motivated by both fundamental and practical interest. The photoionization of Be offers an opportunity to study electron correlation in the simplest multishell atom. The study of ground state photoionization reveals details of the odd parity continua; excited p states, on the other hand, interact with the even parity continua. In addition, photoionization cross sections of Be from both ground and excited states are needed for modeling of astrophysical and fusion plasmas. Moccia and Spizzo [9] studied photoionization of the $Be(2s2p\ ^3P^o)$ state below the $Be^+(2p)$ threshold using variational wave functions. Total photoionization cross sections from the ground and several excited states including $2s2p\ ^{1,3}P^o$ states of Be and Be-like ions were reported by Tully *et al.* [10] as a part of the Opacity Project (OP). They calculated photoionization cross sections over a wide energy range using the OP *R*-matrix codes [15]. We recently carried out an extensive calculation of the partial and total photoionization cross sections and β parameter from the ground state of atomic beryllium [14].

In the present work, we extend our previous photoionization calculations of ground state atomic beryllium [14] to the excited $2s2p\ ^{1,3}P^o$ states, and report partial and total photoionization cross sections of these excited $2s2p\ ^{1,3}P^o$ states. For this detailed study of the doubly excited autoionizing levels from threshold up to the $Be^+(3d)$ threshold, we utilize the enhanced eigenchannel *R*-matrix approach [16–18]. The techniques applied here to describe excited state photoionization are the same as those used previously for ground state atomic beryllium [14] and magnesium [19]. A brief description of these techniques is given in the following section.

II. BRIEF DESCRIPTION OF CALCULATION

We considered the following photoionization processes in the present work:

$$Be(2s2p\ ^{1,3}P^o) + \gamma \rightarrow Be^+(ns\ ^2S) + \epsilon s(^{1,3}S) \quad (1)$$

$$\rightarrow Be^+(ns\ ^2S) + \epsilon d(^{1,3}D) \quad (2)$$

$$\rightarrow Be^+(np\ \ ^2P) + \epsilon p(^{1,3}S,P,D) \quad (3)$$

with $n=2$ and 3 and γ representing the incident photon. The general details of the calculation are given in Ref. [14] and references therein. In brief, the major approximation in this calculational formalism concerns the use of a Hamiltonian H that does not refer to the full atomic system, but represents only the valence electrons plus a central potential to represent the effect(s) of the inner shell [14]. The calculations employ a set of basis functions y_i that consists of all possible products of a set of one-electron orbitals outside the closed shell, as was done for ground state atomic beryllium [14]. A superposition of these orthonormal basis functions is used in a small region inside the *R*-matrix volume of radius r_0 to obtain a variational estimate of the logarithmic derivative of the wave function at a given energy. We have used $r_0 = 20$ a.u. for the current calculations. The calculation of coefficients c_i of the basis functions $\psi_\beta = \Sigma_i c_i^\beta y_i$ is performed by a generalized configuration interaction approach based on the eigenchannel *R*-matrix method [18]. The basis set is divided into open and closed functions in this eigenchannel *R*-matrix approach, depending on their behavior over the reaction surface. The open functions represent only two of the electron orbitals of the many-electron basis functions that are nonzero at the *R*-matrix boundary, while all of the electron orbitals represented by closed functions are zero at the boundary. We have used two open orbitals and 20 closed orbitals for each l ($l \leqslant 5$). We include basis functions representing all possible symmetries resulting from the possible

TABLE I. Ionization thresholds (in eV) relative to ground and excited states of atomic Be.

State	$2s^2\,{}^1S^e$		$2s2p\,{}^3P^o$		$2s2p\,{}^1P^o$	
	[a]	[b]	[a]	[b]	[a]	[b]
$1s^2 2s\,{}^2S$	9.2959	9.3227	6.5728	6.5977	4.0229	4.0453
$1s^2 2p\,{}^2P^o$	13.2543	13.2814	10.5358	10.5564	7.9814	8.0040
$1s^2 3s\,{}^2S$	20.2305	20.2621	17.5074	17.5371	14.9516	14.9847
$1s^2 3p\,{}^2P^o$	21.2688	21.2866	18.5457	18.5616	15.9804	16.0092
$1s^2 3d\,{}^2D$	21.4569	21.4799	18.7264	18.7549	16.1770	16.2025

[a]Present result.
[b]NIST data.

combinations of the one-electron orbitals with $n,m \leqslant 20$, i.e., $(nl,ml+1)$ for ${}^{1,3}P^o$; (nl^2), (nl,ml) for ${}^1S^e$; (nl,ml) for ${}^3S^e$; (nl,ml) for ${}^1P^e$; (nl^2), (nl,ml) for ${}^3P^e$; (nl^2), $(nl,ml+2)$ for ${}^1D^e$; (nl,ml), $(nl,ml+2)$ for ${}^3D^e$. The calculated ionization energies leading to the ionic $Be^+(2s\,{}^2S^e, 2p\,{}^2P^o, 3s\,{}^2S^e, 3p\,{}^2P^o,$ and $3d\,{}^2D^e)$ states relative to the ground state of atomic beryllium are given in Table I. Agreement with experimental values obtained from the NIST data base [20] is seen to be excellent.

The energy-normalized eigenstates ψ_α in each eigenchannel can be represented by a linear combination of the unnormalized eigenstates which, along with the ground state wave function ψ_0, are used to calculate the reduced dipole matrix elements, given in length form as

$$d_\alpha(L) = \langle \psi_\alpha \| \vec{r_1} + \vec{r_2} \| \psi_0 \rangle. \tag{4}$$

The details of the above eigenchannel *R*-matrix formulation are discussed elsewhere [21].

For the calculation of the partial cross sections, we modified the noniterative eigenchannel *R*-matrix code slightly as described in [14], because the previous version used a transformed numerical methodology for efficiency but produced only the total cross section. Recently, this approach has been successfully applied to the calculation of the partial photoionization cross sections in the region above the second ionization threshold for ground state beryllium and magnesium atoms [14,19]. We have also used the same ideas of eigenphase sum gradients as described in [14,19,22] for the calculations of the resonance parameters, such as the resonance energies E_r, effective quantum numbers n^*, and widths Γ.

III. RESULTS AND DISCUSSION

A. Photoionization below the $Be^+(2p\,{}^2P)$ threshold

The photoionization cross sections for ionization to the $Be^+(2s)$ state, the only open channels below the $2p$ threshold of Be^+, from the excited $2s2p\,{}^{1,3}P^o$ states, are shown in Figs. 1(a) and 1(d), along with the associated partial cross sections in Figs. 1(b,c) and 1(e,f) for the singlet and triplet cases, respectively. The length and velocity results, the solid and dotted curves, respectively, are displayed individually. The excellent agreement between the two indicates the accuracy of the calculation. The first, second, and third vertical dotted lines in Figs. 1(a) and 1(d) represent the $Be^+(2p\,{}^2P)$, $Be^+(3s\,{}^2S)$, and $Be^+(3p\,{}^2P)$ ionization thresholds. As shown in Fig. 1, the features of the photoionization spectra for each of the singlet and triplet processes differ in several aspects.

In the energy region below the $Be^+(2p)$ threshold, the background (nonresonant) cross sections for photoionization of ${}^1P$ and ${}^3P$ initial states are roughly equal. In this energy region there are three Rydberg series in the triplet manifold and three in the singlet, each converging to the $Be^+(2p)$ threshold, for the photoionization of the excited $2s2p\,{}^{1,3}P^o$ states. The ${}^1P^o \rightarrow {}^1S^e$ cross section $\sigma_{2s\epsilon s\,{}^1S}$, showing the $2pnp\,{}^1S$ Rydberg series, is seen in Fig. 1(b); the ${}^1P^o \rightarrow {}^1D^e$ cross section $\sigma_{2s\epsilon d\,{}^1D}$, showing the $2pnp\,{}^1D$ and $2pnf\,{}^1D$ Rydberg series in Fig. 1(c). The analagous triplet cross sections, with the associated resonances, are presented in Figs. 1(e) and 1(f), respectively. The lower members of these series are identified in Table II. The photoionization cross section leading to the $Be^+(2s)$ state from ${}^1P$ shown in Fig. 1(a) is, of course, the sum of Figs. 1(b) and 1(c), while the cross section from ${}^3P^o$ shown in Fig. 1(d) is the sum of Figs. 1(e) and 1(f). Except for the resonances the cross sections are seen to be dominated by the $p \rightarrow d$ channel $(2s\epsilon d)$, in each case, by more than an order of magnitude over the $p \rightarrow s$ $(2s\epsilon s)$ channel.

The resonances have been studied in detail and their energy positions E_r, effective quantum numbers n^*, and widths Γ are given in Table II. The strongest resonance [cf, Fig. 1(b)] is the $2p^2\,{}^1S$ resonance, just above threshold for ${}^1P^o$ photoionization. This is clearly because it results from a one-electron $\Delta n = 0$ transition since the dipole matrix element is rather large when initial and final states occupy the same region of space. The $2p^2\,{}^1D^e$ is not seen because it lies below threshold [23], and the ${}^3P^e$ is also a real bound state because there is no ${}^3P$ continuum for it to decay into.

It is also seen from Fig. 1 and Table II that the $2pnp\,{}^1S$ resonances are an order of magnitude wider than the $2pnp\,{}^3S$; and the $2pnp\,{}^1D$ resonances are two orders of magnitude larger than the corresponding $2pnp\,{}^3D$. This is because in the singlet manifold, since the spatial part of the wave function is symmetric, the direct and exchange terms add, while for the triplet manifold, with antisymmetric spatial wave function, they are of opposite sign and partially cancel. For the ${}^3D$ resonances, in particular, the cancellation is almost complete, so that the ${}^3D$ resonances are narrower than the ${}^3S$, while the ${}^1D$ resonances are wider than the ${}^1S$. That it is the $2pnp\,{}^3D$ series that is anomalous, owing to the

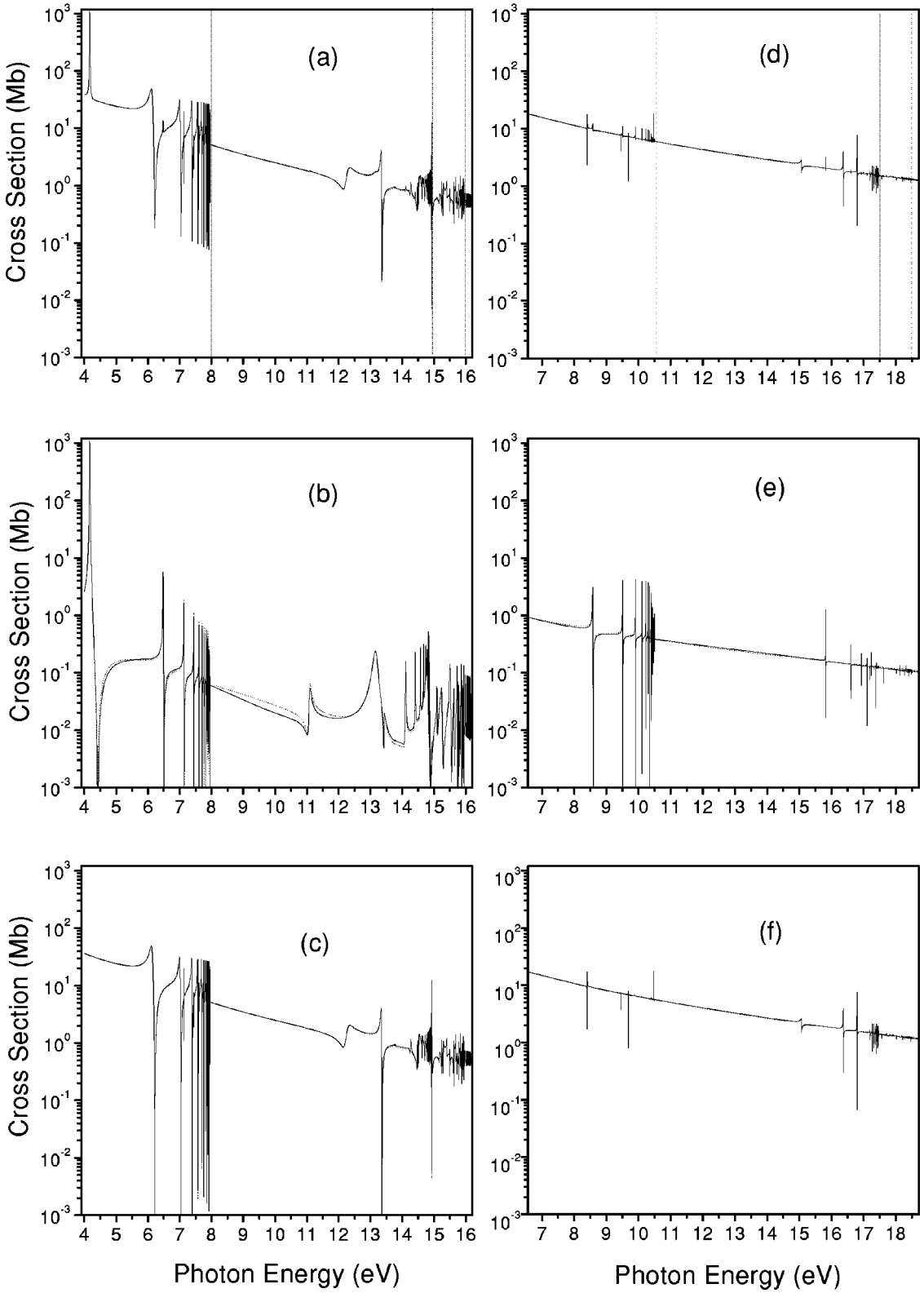

FIG. 1. (a) Photoionization cross sections leading to the $Be^+(2s)$ state from the excited $2s2p\ ^1P^o$ states as a function of photon energy; (b) $\sigma_{2s\epsilon s\ ^1S}$;(c) $\sigma_{2s\epsilon d\ ^1D}$; (d) photoionization cross sections leading to the $Be^+(2s)$ state from the excited $2s2p\ ^3P^o$ states as a function of photon energy; (e) $\sigma_{2s\epsilon s\ ^3S}$;(f) $\sigma_{2s\epsilon d\ ^3D}$. Solid curves, present length results; dotted curves, present velocity results. The vertical dotted lines represent the $Be^+(2p,3s,and 3p)$ thresholds, respectively.

TABLE II. Resonance positions (E_r in eV), effective quantum numbers (n^*), and widths (Γ in eV) of autoionizing levels converging to the $Be^+(2p)$ threshold.

	$2pnp\ ^1S$			$2pnp\ ^1D$			$2pnf\ ^1D$		
n	E_r	n^*	Γ	E_r	n^*	Γ	E_r	n^*	Γ
2	4.2065	1.8985	0.0821						
3	6.4795	3.0098	0.0241	6.1423	2.7199	0.1003			
4	7.1350	4.0094	0.0073	7.0055	3.7339	0.0441	7.1450	4.0332	0.0005
5	7.4401	5.0137	0.0042	7.3755	4.7388	0.0200	7.4446	5.0346	0.0003
6	7.6054	6.0161	0.0027	7.5685	5.7404	0.0108	7.6077	6.0338	0.0001
7	7.7052	7.0186	0.0017	7.6820	6.7411	0.0065	7.7064	7.0337	
8	7.7698	8.0202	0.0013	7.7544	7.7417	0.0042	7.7707	8.0339	
9	7.8142	9.0208	0.0009	7.8034	8.7421	0.0029	7.8147	9.0339	
10	7.8459	10.0215	0.0008	7.8380	9.7407	0.0003	7.8462	10.0328	
11	7.8694	11.0223	0.0006	7.8635	10.7413	0.0003	7.8696	11.0327	
12	7.8872	12.0215	0.0005	7.8827	11.7394	0.0002	7.8874	12.0326	
	$2pnp\ ^3S$			$2pnp\ ^3D$			$2pnf\ ^3D$		
n	E_r	n^*	Γ	E_r	n^*	Γ	E_r	n^*	Γ
3	8.5871	2.6423	0.0069	8.4157	2.5333	0.0006			
4	9.5127	3.6467	0.0039	9.4588	3.5543	0.0004	9.6968	4.0269	0.0012
5	9.9076	4.6539	0.0019	9.8820	4.5619	0.0002	9.9982	5.0308	0.0006
6	10.1107	5.6575	0.0011	10.0968	5.5671	0.0001	10.1618	6.0317	0.0002
7	10.2290	6.6595	0.0007	10.2205	6.5690		10.2608	7.0334	0.0001
8	10.3040	7.6608	0.0005	10.2983	7.5682		10.3249	8.0323	
9	10.3544	8.6612	0.0003	10.3505	8.5682		10.3690	9.0313	
10	10.3900	9.6615	0.0003	10.3872	9.5694		10.4006	10.0319	
11	10.4161	10.6615	0.0002	10.4140	10.5686		10.4240	11.0302	
12	10.4358	11.6614	0.0002	10.4342	11.5678		10.4418	12.0306	

cancellation, is further evident from the line profiles; the $2pnp\ ^1D, ^1S$, and ^3S series all show positive q values, while for the $2pnp\ ^3D$ it is negative. The $2pnf$ series is very weak in both singlet and triplet cases, the resonances being very narrow and exhibiting a negative q value.

TABLE III. Photoelectron energy (in eV) of resonances converging to the $Be^+(2p)$ threshold compared with other calculations.

State	E_r[a]	E_r[b]	E_r[c]
$2p3p\ ^3S$	2.0118	1.9973	2.0735
$2p4p\ ^3S$	2.9378		2.9838
$2p5p\ ^3S$	3.3326		3.3732
$2p^2\ ^1S$	0.1836	1.0531	0.1897
$2p3p\ ^1S$	2.4566	2.5089	2.4953
$2p4p\ ^1S$	3.1121		3.1557
$2p3p\ ^3D$	1.8537		1.8790
$2p4p\ ^3D$	2.8870		2.9334
$2p3p\ ^1D$	2.1170		2.1533
$2p4p\ ^1D$	2.9816		3.0365
$2p4f\ ^3D$	3.1240		3.1669
$2p4f\ ^1D$	3.1221		3.1696

[a]Present result.
[b]Lin [6].
[c]Moccia and Spizzo [9].

The present results are compared in Table III with the results of other calculations. There is good agreement between various calculations except for the position of the $2p^2\ ^1S$ resonance, which is very sensitive to correlation. Our result for this resonance agrees well with that of Ref. [9]. In our calculation it is positioned about 0.18 eV above the threshold. In the OP calculation of Tully *et al.* [10] it lies approximately 0.32 eV above threshold. The tables of Moore [23] and of Fawcett [24] show it to lie below threshold as a bound state. However, the experiment of Beigang *et al.* [25] agrees with the present theoretical predictions and shows that this state lies above threshold. It is clear from Table II that all of these series display smooth regular behavior with approximately constant quantum defects except for $2p^2\ ^1S$, the lowest member of the $2pnp\ ^1S$ series.

B. Photoionization between the $Be^+(2p\ ^2P)$ and $Be^+(3s\ ^2S)$ thresholds

The photoionization cross sections leading to the $Be^+(2p)$ state from the excited $2s2p\ ^{1,3}P^o$ states are shown in Figs. 2(a) and 2(f), respectively. The partial cross sections $\sigma_{2p\epsilon p\ ^1S,\ ^1P,\ ^1D}$ and $\sigma_{2p\epsilon f\ ^1D}$ for singlet processes are shown in Figs. 2(b–e), while corresponding cross sections for triplet cases are shown in Figs. 2(g–j).

Along with the $2s\epsilon s\ ^{1,3}S^e$ and $2s\epsilon d\ ^{1,3}D^e$ channels that are already open, the $2p\epsilon p\ ^{1,3}S^e, P^e, D^e$ and $2p\epsilon f\ ^{1,3}D^e$

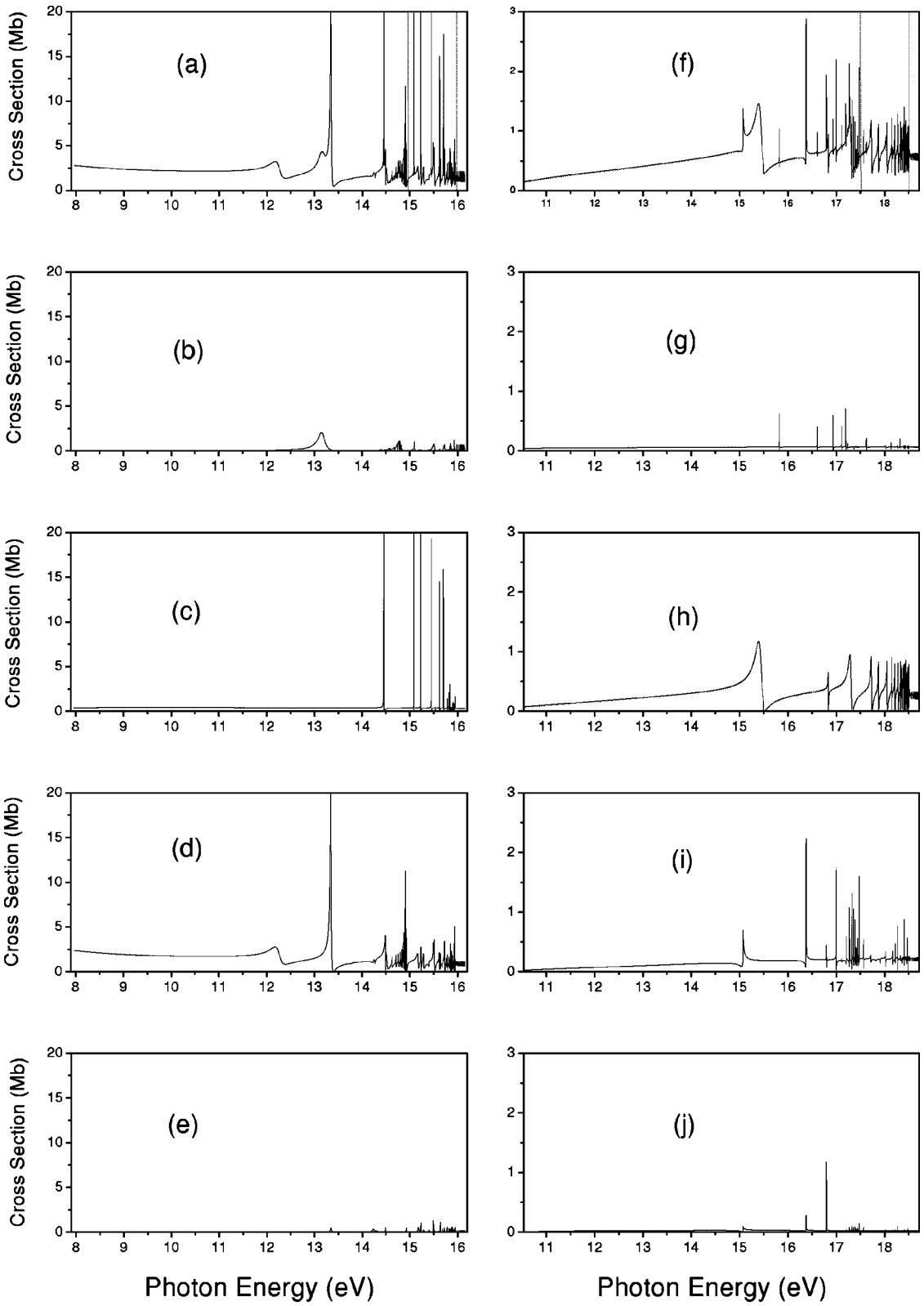

FIG. 2. (a) Photoionization cross sections leading to the $Be^+(2p)$ state from the excited $2s2p\ ^1P^o$ states as a function of photon energy; (b) $\sigma_{2p\epsilon p\ ^1S}$; (c) $\sigma_{2p\epsilon p\ ^1P}$;(d) $\sigma_{2p\epsilon p\ ^1D}$; (e) $\sigma_{2p\epsilon f\ ^1D}$;(f) photoionization cross sections leading to the $Be^+(2p)$ state from the excited $2s2p\ ^3P^o$ states as a function of photon energy; (g) $\sigma_{2p\epsilon p\ ^3S}$; (h) $\sigma_{2p\epsilon p\ ^3P}$;(i) $\sigma_{2p\epsilon p\ ^3D}$; (j) $\sigma_{2p\epsilon f\ ^3D}$. Solid curves, present length results; dotted curves, present velocity results. The vertical dotted lines represent the Be^+ (3*s* and 3*p*)‘ thresholds, respectively.

TABLE IV. Resonance positions (E_r in eV), effective quantum numbers (n^*), and widths (Γ in eV) of autoionizing levels converging to the $Be^+(3s)$ threshold.

	$3sns\ ^1S$			$3sns\ ^3S$		
n	E_r	n^*	Γ	E_r	n^*	Γ
3	11.0909	1.8773	0.1439			
4	13.4417	3.0018	0.0488	15.8362	2.8533	0.0017
5	14.1060	4.0113	0.0266	16.6077	3.8887	0.0013
6	14.4098	5.0111	0.0162	16.9377	4.8870	0.0010
7	14.5743	6.0052	0.0152	17.1088	5.8426	0.0008
8	14.6735	6.9945	0.0104	17.1991	6.6424	0.0008
9	14.7379	7.9794	0.0113	17.2500	7.2703	0.0002
10	14.7827	8.9740	0.0159	17.3428	9.0920	0.0005
11	14.8187	10.1190	0.0115	17.3740	10.0974	0.0004
12	14.8413	11.1081	0.0038	17.4108	11.8636	0.0002
			$3snd\ ^1D$			$3snd\ ^3D$
n	E_r	n^*	Γ	E_r	n^*	Γ
3	12.2068	2.2264	0.2570	15.0702	2.3627	0.0235
4	13.7992	3.4360	0.0347	16.3922	3.4929	0.0038
5	14.2340	4.3542	0.0455	16.8112	4.4205	0.0011
6	14.5233	5.6363	0.0593	17.0110	5.2349	0.0009
7	14.6282	6.4854	0.0078	17.1247	5.9620	0.0020
8	14.7086	7.4829	0.0040	17.2796	7.7270	0.0007
9	14.7624	8.4791	0.0025	17.3305	8.7703	0.0011
10	14.8001	9.4752	0.0017	17.3647	9.7627	0.0004
11	14.8276	10.4734	0.0012	17.3909	10.8063	0.0004
12	14.8482	11.4706	0.0010	17.4108	11.8636	0.0002

channels open above the $Be^+(2p)$ threshold. Thus, the $^{1,3}S$ and $^{1,3}D$ manifolds of final continuum states can branch to either $Be^+(2s)$ or $Be^+(2p)$ channels, but the $^{1,3}P$ manifold can lead only to the $Be^+(2p)$ channel.

Looking first at the background (nonresonant) cross sections, it is evident from Figs. 1 and 2 that between the $Be^+(2p\ ^2P)$ and $Be^+(3s\ ^2S)$ thresholds the cross section for producing the $Be^+(2s)$ state ($2p$ ejection) is larger for the ^3P initial state than for the ^1P, as seen in Figs. 1(a) and 1(d). On the other hand, for producing the $Be^+(2p)$ state ($2s$ ejection), the ^1P cross section is considerably larger than the ^3P, as shown in Figs. 2(a) and 2(f). Furthermore, just above the $Be^+(2p)$ threshold, the cross section for producing $Be^+(2s)$ ($2p$ ejection) dominates for both singlet and triplet initial states; but at higher energies the cross sections for producing the two possible final states of Be^+, $2s$ and $2p$, become more competitive because the $Be^+(2s)$ production cross section ($2p$ ejection) falls off more rapidly with energy than the $2s$ ejection cross section [which leads to $Be^+(2p)$ production].

As seen in Fig. 1 for $Be^+(2s)$ production, in this energy region too both the singlet and triplet cross sections are dominated by the $p\rightarrow d$ ($2s\epsilon d$) channels by more than an order of magnitude over the $p\rightarrow s$ ($2s\epsilon s$) channel. From Fig. 2 for $Be^+(2p)$ production, a complicated pattern emerges. There are three $2p\epsilon p$ channels, in each case, along with a very small $2p\epsilon f$ channel, which total to the $Be^+(2p)$ production cross section. From (angular momentum) geometry, the cross sections for $2p\epsilon p$ $^{1,3}S$, $^{1,3}P$, and $^{1,3}D$ channels should be in a the ratio of 1:3:5. Clearly, that is not the case. For the singlet initial state, $\sigma_{2p\epsilon p\ ^1D}$ [Fig. 2(d)] dominates, while, for the triplet case, $\sigma_{2p\epsilon p\ ^3P}$ [Fig. 2(h)] is largest. Thus, dynamical effects on the various continuum multiplets are extremely important; in the near-threshold region, these dynamical effects are provided principally by the differences in the exchange interaction between the continuum ϵp electron and the ion core among the different multiplets.

The resonance patterns are significantly more complicated in this energy region than in the region below the $Be^+(2p)$ threshold. This is because, although there are only two series of resonances converging to the $Be^+(3s)$ threshold for each initial state, there are interlopers appearing which are the lower members of resonant series converging to $Be^+(3p)$ and even $Be^+(3d)$. This occurs because the $Be^+ n=3$ thresholds are so close in energy.

Analysis of the resonances arising from both the ^1P and ^3P initial states coverging to the $Be^+(3s)$ threshold, shown in Table IV, clearly indicates the presence of interlopers by the sudden changes in quantum defect, and anomalies in width, in going along a given series. For example, between the $3s5d\ ^1D$ and $3s6d\ ^1D$ resonances lie $3p4p\ ^1D$ at 14.2689 eV and $3d4s\ ^1D$ at 14.4905 eV. Thus, the quantum defects and widths change dramatically in this energy region.

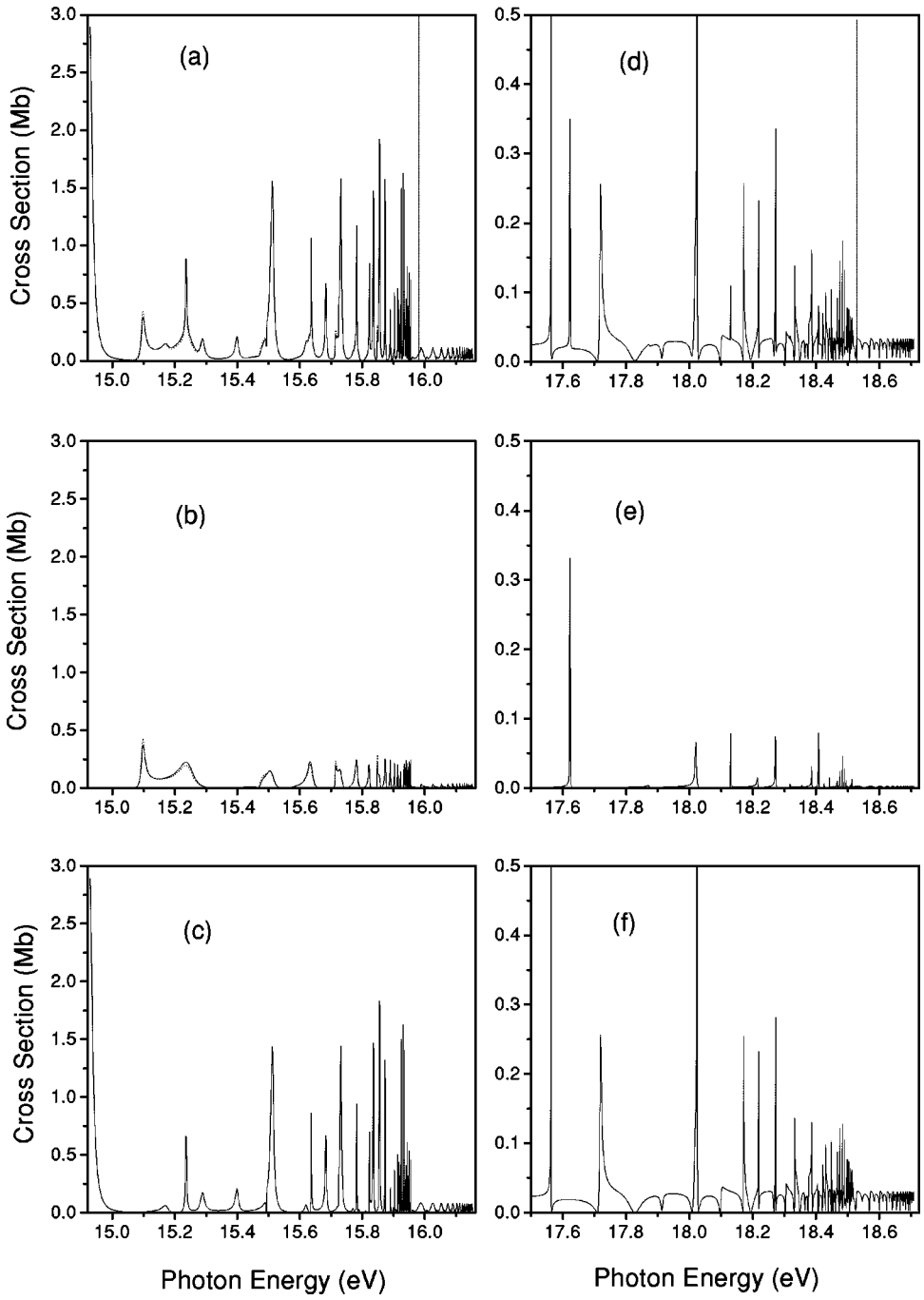

FIG. 3. (a) Photoionization cross sections leading to the $Be^+(3s)$ state from the excited $2s2p\ ^1P^o$ states as a function of photon energy; (b) $\sigma_{3s\epsilon s\ ^1S}$; (c) $\sigma_{3s\epsilon d\ ^1D}$; (d) photoionization cross sections leading to the $Be^+(3s)$ state from the excited $2s2p\ ^3P^o$ states as a function of photon energy; (e) $\sigma_{3s\epsilon s\ ^3S}$; (f) $\sigma_{3s\epsilon d\ ^3D}$. Solid curves, present length results; dotted curves, present velocity results. The vertical dotted line represents the $Be^+(3p)$ threshold.

In addition to the interlopers that perturb the $3sns\ ^{1,3}S$ and $3snd\ ^{1,3}D$ series, there are interlopers that are not close enough to any of these resonances to significantly perturb them, but which still alter the resonance pattern considerably, owing to their strength. As an example, the $3p^2\ ^1D$ resonance at about 13.35 eV shows up very strongly in Figs. 1(c) and 2(d) and dominates the energy region. Similarly, the broad ^3P resonance just below 15.5 eV [Fig. 2(h)], which dominates the triplet cross section in that energy region, is the $3p^2\ ^3P$ resonance.

As in the case of the resonances leading up to the $Be^+(2p)$, the widths of the singlet resonances are seen (Table IV) to be about an order of magnitude larger than their triplet counterparts; and this occurs for the same reason as in the previous case. Further, the $^{1,3}S$ resonances are somewhat wider than the corresponding $^{1,3}D$ resonances, again like the previous case.

C. Photoionization between the $Be^+(3s\ ^2S)$ and $Be^+(3p\ ^2P)$ thresholds

In this energy region, the channels leading to the $Be^+(3s\ ^2S)$ state open, in addition to the channels already open. The total photoionization cross sections for the singlet and triplet initial states are shown in Figs. 3(a) and 3(d), respectively, while the partial cross sections are shown in Figs. 3(b,c) and 3(e,f), respectively. These cross sections are

fundamentally different from the ones discussed in the previous sections in one very important way: Photoionization to the $Be^+(2s\,^2S)$ or $Be^+(2p\,^2P)$ are single-electron transitions, predominantly $2p \rightarrow \epsilon s,d$ or $2s \rightarrow \epsilon p$. Photoionization to the $Be^+(3s\,^2S)$ state, on the other hand, requires a two-electron transition, i.e., photoionization plus excitation. This two-electron process is much less likely than a single-electron transition; consequently, it is expected that the cross section will be extremely small. From Fig. 3, it is evident that it is indeed the case. On the scales shown, the nonresonant continuum cross sections are too small to appear. Thus, the strength of the $Be^+(3s\,^2S)$ cross sections, from both singlet and triplet states, is almost entirely due to resonances in the newly opened $Be^+(3s)$ channels.

The resonance structure in this region gets even more complex owing to the very small energy difference, ~ 0.2 eV, between the $3p$ and $3d$ thresholds of Be^+. This is evident from Table V where the details of the four resonant singlet and four resonant triplet series converging on the $Be^+(3p\,^2P)$ state are given and quite a number of anomalies are seen in the quantum defects and widths in virtually every series owing to interlopers from the lower (and not so lower) members of series converging on $Be^+(3d\,^2D)$. As was the case previously, the singlet series are wider than the triplets, with one exception. Aside from series perturbations caused by interlopers, the members of the $3pnp\,^3P$ series are wider than the corresponding ^1P resonances; this is abundantly clear from Figs. 2(c) and 2(h).

A peculiar feature is noted in the $Be^+(3s)$ cross section just at theshold in the case of the final ^1D state, seen in Figs. 3(a) and 3(c); there is a structure that is fairly high ($\sim$ 3 Mb) and decreasing from threshold. Since this is a two-electron ionization plus excitation channel, that is far too large for the nonresonant background cross section, as discussed above. It turns out to be caused by the $3d^2\,^1D$ resonance which is quite strong and straddles the threshold. The centroid of the resonance lies at about 14.93 eV, $\sim$ 0.03 eV below the threshold, but its width is approximately 0.04 eV (see Table VI) so it overlaps the threshold.

D. Photoionization between the $Be^+(3p\,^2P)$ and $Be^+(3d\,^2D)$ thresholds

The cross sections for photoionization leading to production of $Be^+(3p\,^2P)$ from both singlet and triplet initial states are shown in Fig. 4. It is evident from the figure that for both singlet and triplet cases the background (nonresonant) cross sections are tiny, too small to appear on the scale of the figure. In the total $Be^+(3p)$ cross section, in each case, there appears to be a background, but closer scrutiny reveals that this apparent background is simply the sum of the various resonant series, Figs. 4(b–e) for the singlet case and Figs. 4(g–j) for the triplet. The background cross sections are so small for exactly the same reason as discussed in the previous section for the $Be^+(3s\,^2S)$ cross sections; these channels represent two-electron ionization plus excitation processes. There are four series of resonances leading up to the $Be^+(3d)$ threshold in the singlet case, $3dnd\,^1S,^1P,^1D$, and

TABLE V. Resonance positions (E_r in eV), effective quantum numbers (n^*), and widths (Γ in eV) of autoionizing levels converging to the $Be^+(3p)$ threshold.

	$3pnp\,^1S$			$3pnp\,^3S$		
n	E_r	n^*	Γ	E_r	n^*	Γ
3	13.1742	2.2019	0.3526			
4	14.8916	3.5349	0.0007	17.3012	3.3065	0.0014
5	15.2507	4.3180	0.1132	17.6155	3.8245	0.0040
6	15.5118	5.3881	0.0542	18.0254	5.1137	0.0086
7	15.6342	6.2688	0.0404	18.1292	5.7153	0.0040
8	15.7332	7.4191	0.0268	18.2767	7.1118	0.0026
9	15.7821	8.2825	0.0193	18.3209	7.7800	0.0013
10	15.8212	9.2442	0.0116	18.3914	9.3910	0.0034
11	15.8569	10.4960	0.0116	18.4131	10.1308	0.0007
12	15.8741	11.3099	0.0089	18.4314	10.9082	0.0002
	$3pnp\,^1P$			$3pnp\,^3P$		
n	E_r	n^*	Γ	E_r	n^*	Γ
3				15.3888	2.0760	0.2667
4	14.4641	2.9955	0.0030	17.3039	3.3100	0.0505
5	15.2331	4.2668	0.0003	17.8739	4.5001	0.0055
6	15.4541	5.0842	0.0008	18.1522	5.8801	0.0018
7	15.6279	6.2181	0.0004	18.2143	6.4079	0.0044
8	15.7087	7.0759	0.0047	18.3296	7.9350	0.0013
9	15.7807	8.2544	0.0047	18.3567	8.4847	0.0016
10	15.8190	9.1815	0.0005	18.4135	10.1465	0.0024
11	15.8462	10.0674	0.0004	18.4327	10.9712	0.0019
12	15.8745	11.3329	0.0004	18.4454	11.6477	0.0007
	$3pnp\,^1D$			$3pnp\,^3D$		
n	E_r	n^*	Γ	E_r	n^*	Γ
3	13.3495	2.2741	0.0285			
4	14.2689	2.8195	0.0164	17.2142	3.1967	0.0014
5	15.2873	4.4304	0.0117	17.7244	4.0701	0.0107
6	15.5129	5.3944	0.0101	18.0311	5.1418	0.0012
7	15.6243	6.1809	0.0083	18.2249	6.5126	0.0006
8	15.7324	7.4072	0.0048	18.2800	7.1540	0.0004
9	15.7893	8.4367	0.0029	18.3544	8.4334	0.0097
10	15.8226	9.2836	0.0010	18.3946	9.4902	0.0016
11	15.8557	10.4445	0.0020	18.4162	10.2477	0.0008
12	15.8735	11.2796	0.0005	18.4462	11.6926	0.0028
	$3pnf\,^1D$			$3pnf\,^3D$		
n	E_r	n^*	Γ	E_r	n^*	Γ
4	15.1685	4.0937	0.0253	17.5659	3.7264	0.0001
5	15.3983	4.8347	0.0157	18.0190	5.0824	0.0132
6	15.5947	5.9388	0.0064	18.1802	6.1008	0.0024
7	15.6841	6.7758	0.0056	18.2752	7.0916	0.0042
8	15.7700	8.0407	0.0045	18.3410	8.1525	0.0020
9	15.8102	8.9406	0.0038	18.3842	9.1780	0.0025
10	15.8359	9.7029	0.0022	18.4132	10.1325	0.0005
11	15.8719	11.1961	0.0021	18.4391	11.2944	0.0010
12	15.8851	11.9469	0.0015	18.4567	12.3655	0.0006

$3dns\ ^1D$, along with the corresponding four series in the triplet case. The details of the resonant series are given in Table VI. Many of the lower members of each of the series lie below $Be^+(3p\ ^2P)$ and a few even below $Be^+(3s\ ^2S)$; this is a consequence of the fact that the $n=3$ thresholds are so close together in energy.

Owing to the overlapping of the various series of resonances converging on $Be^+(3d)$ with the series converging to the two lower thresholds of Be^+, there is no regularity in the parameters of the lower members of the various series of resonances detailed in Table VI. However, for the parts of the series that lie *above* the $Be^+(3p)$ threshold, there are no more overlapping series converging to different limits; the lowest members of the next resonance series, those converging to $Be^+(4s)$, are higher in energy. Thus, it is expected that above the $Be^+(3p)$ threshold, the parameters of the series converging to $Be^+(3d)$ will behave smoothly. This is exactly what is observed in Table VI.

E. Total photoionization cross sections

The total photoionization cross sections for the photoionization of the excited $2s2p\ ^{1,3}P^o$ states of atomic beryllium are obtained by adding respective partial cross sections. The present and the OP results [10] for the total photoionization cross sections of the excited $2s2p\ ^1P^o$ and $2s2p\ ^3P^o$ states are shown in Fig. 5. Our results show rather good overall agreement with the OP results. The resonance structure in the OP calculation is slightly shifted to the higher energy side with respect to our results owing to a slight difference in the threshold energies in the two calculations. Some of the resonances are also rather different, e.g., the near-threshold resonance in the ^1P case, which the present calculation finds much closer to threshold and an order of magnitude stronger. Numerous other differences in resonance strengths are seen in the figure, particularly in the ^3P case.

But the largest differences accrue above the $Be^+(3s)$ thresholds because the OP calculations made the simplifying approximation that all of the $n=3$ thresholds of Be^+ were at the same energy. From the discussion of the previous sections, it is clear that such an approximation renders the OP resonance structure in this energy region completely unphysical since interacting resonant series were seen to dominate the phenomenology there.

Both ^1P and ^3P total photoionization cross sections are seen to be dominated by Rydberg series of autoionizing resonances converging to the various ionic thresholds. However, the resonances are much stronger in the singlet case, as opposed to the triplet case, as seen in Fig. 5. This could be due to the fact that for the singlet states the spatial parts of the two-electron wave functions are symmetric, so that the electrons are, on the average, closer together than in the triplet case where the wave functions are antisymmetric. And, in situations where the electrons are closer together, it would be expected that they interact (correlate) more strongly; such an interaction is required to excite the various doubly excited resonances.

IV. CONCLUSIONS

Calculations of partial and total photoionization spectra for the excited $2s2p\ ^{1,3}P$ states of atomic beryllium between

TABLE VI. Resonance positions (E_r in eV), effective quantum numbers (n^*), and widths (Γ in eV) of autoionizing levels converging to the $Be^+(3d)$ threshold.

	$3dnd\ ^1S$			$3dnd\ ^3S$		
n	E_r	n^*	Γ	E_r	n^*	Γ
3	14.8187	3.1650	0.0115			
4	15.0929	3.5428	0.0394	17.3427	3.1357	0.0337
5	15.4717	4.3923	0.0315	17.8671	3.9791	0.0306
6	15.7117	5.4076	0.0100	18.2187	5.1765	0.0105
7	15.8471	6.4226	0.0038	18.3611	6.1029	0.0040
8	15.9282	7.3957	0.0014	18.4477	6.9873	0.0010
9	15.9873	8.4708	0.0080	18.5092	7.9148	0.0005
10	16.0254	9.4738	0.0067	18.5491	8.6798	0.0198
11	16.0539	10.4801	0.0023	18.5835	9.7584	0.0140
12	16.0744	11.4830	0.0021	18.6112	10.8651	0.0102
	$3dnd\ ^1P$			$3dnd\ ^3P$		
n	E_r	n^*	Γ	E_r	n^*	Γ
3				16.8353	2.6823	0.0045
4	15.0643	3.4936	0.0010	17.7320	3.6990	0.0176
5	15.5335	4.5982	0.0014	18.0545	4.4998	0.0134
6	15.7410	5.5866	0.0318	18.2855	5.5553	0.0054
7	15.8606	6.5576	0.0169	18.4135	6.5946	0.0024
8	15.9333	7.4720	0.0002	18.4842	7.4949	0.0015
9	15.9911	8.5560	0.0119	18.5177	8.0734	0.0022
10	16.0280	9.5560	0.0085	18.5617	9.0902	0.0077
11	16.0549	10.5538	0.0041	18.5947	10.1633	0.0056
12	16.0749	11.5560	0.0032	18.6191	11.2613	0.0042
	$3dns\ ^1D$			$3dns\ ^3D$		
n	E_r	n^*	Γ	E_r	n^*	Γ
4	14.4905	2.8404	0.0021	17.3221	3.1126	0.0003
5	15.4931	4.4604	0.0028	17.5038	3.3359	0.0000
6	15.7242	5.4818	0.0017	17.8223	3.8792	0.0586
7	15.8517	6.4675	0.0008	18.1802	4.9907	0.0024
8	15.9347	7.4949	0.0002	18.3706	6.1837	0.0017
9	15.9861	8.4432	0.0199	18.4601	7.1479	0.0038
10	16.0244	9.4444	0.0144	18.5329	8.3854	0.0012
11	16.0534	10.4712	0.0098	18.5686	9.2870	0.0032
12	16.0739	11.4858	0.0075	18.6000	10.3746	0.0023
	$3dnd\ ^1D$			$3dnd\ ^3D$		
n	E_r	n^*	Γ	E_r	n^*	Γ
3	14.9216	3.3032	0.0366			
4	15.2316	3.7937	0.0041	17.4480	3.2623	0.0001
5	15.6243	4.9617	0.0083	17.7244	3.6849	0.0107
6	15.7822	5.8711	0.0010	18.1011	4.6645	0.0114
7	15.9004	7.0137	0.0016	18.3101	5.7166	0.0049
8	15.9633	7.9798	0.0001	18.4283	6.7551	0.0018
9	16.0055	8.9086	0.0033	18.4973	7.7061	0.0005
10	16.0384	9.9088	0.0025	18.5458	8.6799	0.0053
11	16.0627	10.9050	0.0020	18.5835	9.7584	0.0037
12	16.0807	11.9082	0.0018	18.6106	10.8401	0.0028

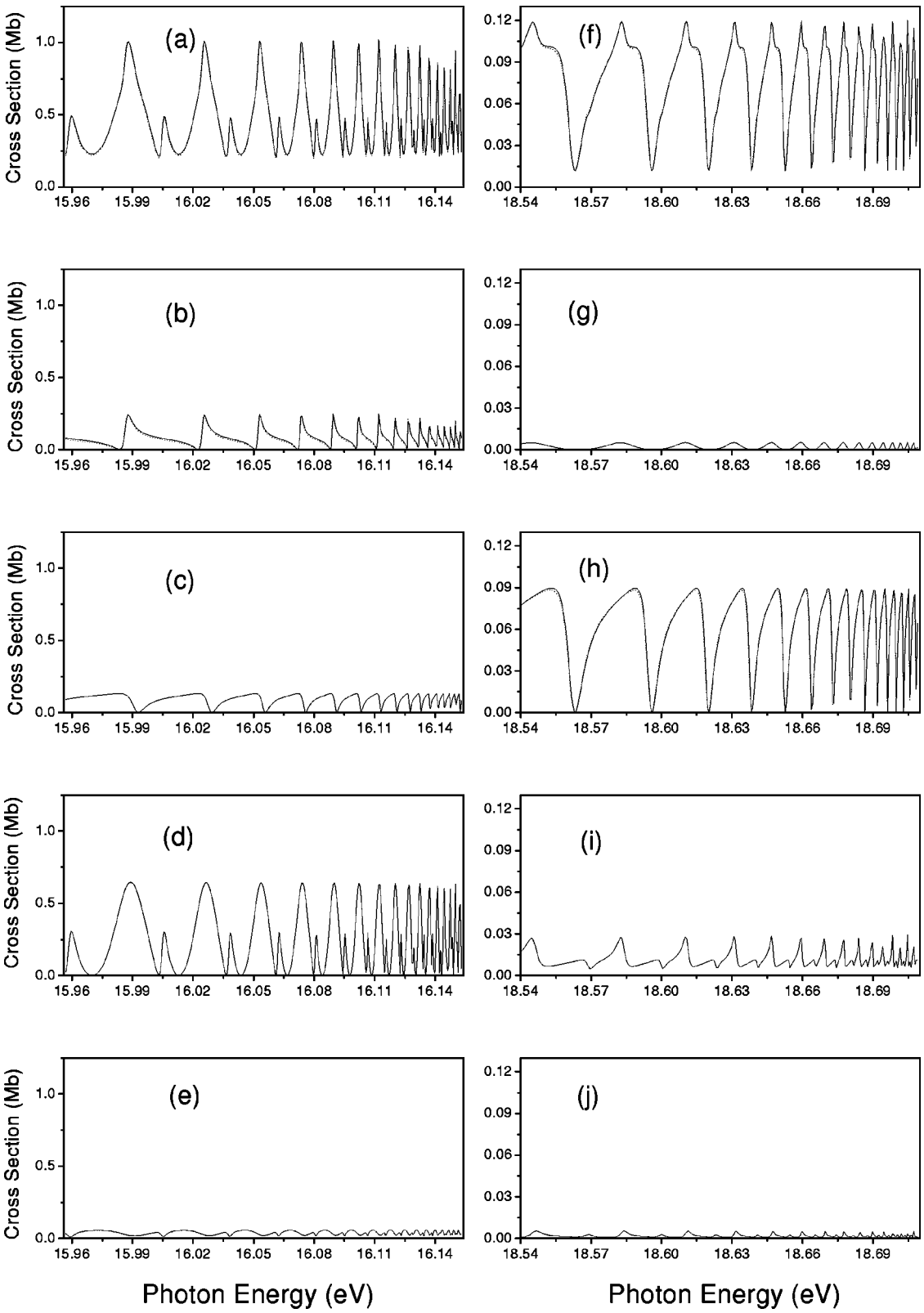

FIG. 4. (a) Photoionization cross sections leading to the $Be^+(3p)$ state from the excited $2s2p\ ^1P^o$ states as a function of photon energy; (b) $\sigma_{3p\epsilon p\ ^1S}$; (c) $\sigma_{3p\epsilon p\ ^1P}$;(d) $\sigma_{3p\epsilon p\ ^1D}$; (e) $\sigma_{3p\epsilon f\ ^1D}$; (f) photoionization cross sections leading to the $Be^+(3p)$ state from the excited $2s2p\ ^3P^o$ states as a function of photon energy; (g) $\sigma_{3p\epsilon p\ ^3S}$;(h) $\sigma_{3p\epsilon p\ ^3P}$; (i) $\sigma_{3p\epsilon p\ ^3D}$;(j) $\sigma_{3p\epsilon f\ ^3D}$. Solid curves, present length results; dotted curves, present velocity results.

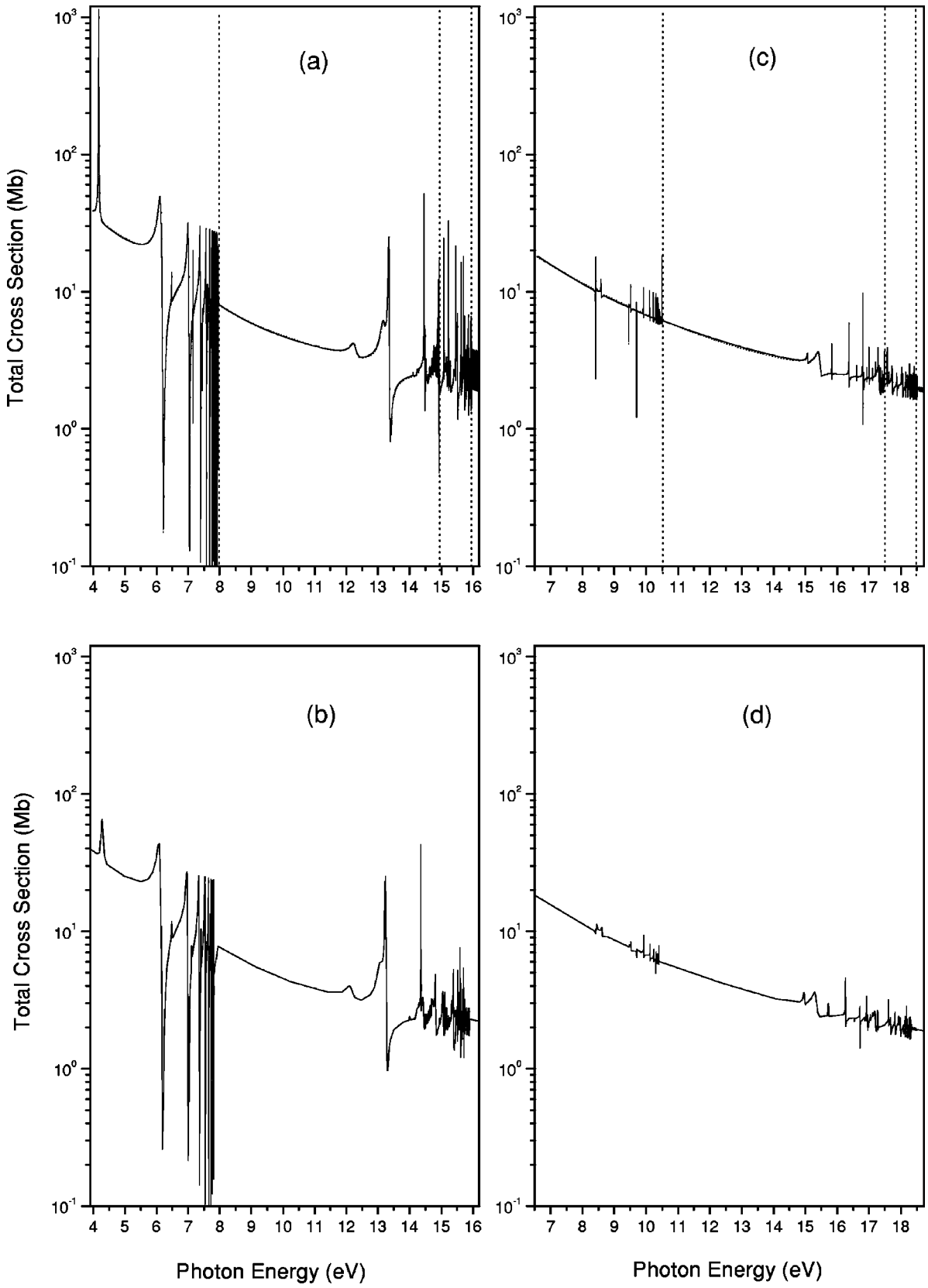

FIG. 5. Total photoionization cross sections for the excited $2s2p\ ^{1,3}P^o$ states of Be as a function of photon energy. (a) Present results for $^1P^o$: solid curve, present length; dashed, present velocity. (b) OP result for $^1P^o$. (c) Present results for $^3P^o$: solid curve, present length; dashed, present velocity. (d) OP result for $^3P^o$. The vertical dotted lines represent the $Be^+(2p,3s$ and $3p)$ thresholds, respectively.

the $Be^+(2s\,^2S)$ and $Be^+(3d\,^2D)$ thresholds using an upgraded eigenchannel *R*-matrix formalism are presented. These calculations are the most accurate and extensive to date, to our knowledge, for the photoionization of the first two excited states of atomic Be. The cross sections are dominated by Rydberg series of autoionizing resonances converging to the various ionic thresholds, particularly for the ^1P initial state. While the background (nonresonant) cross sections are similar both qualitatively and quantitatively for the two initial states, the resonances are quite different. This indicates that dynamical effects, effects due to differing intial and final state wave functions, in the singlet and triplet channels are of great importance.

All of the resonance series up to those converging to the $Be^+(3d\,^2D)$ state were classified, a nontrivial matter due to the overlapping of the various series in the neighborhood of the $n=3$ thresholds. The untangling of these seemingly chaotic regions would not have been possible without the use of a methodology based on eigenphase sum gradients [14,19,22].

Agreement with previous calculations is excellent qualitatively and relatively good quantitatively (with some exceptions) for the background cross section and the resonances leading up to the first excited state of Be^+; for the higher resonances, there is no previous accurate calculation to compare with, but it is expected that the level of accuracy of the present calculation is no different for these resonances than for the lower ones. Experimental studies would be highly desirable to confirm our understanding of the physics of these photoionization processes.

ACKNOWLEDGMENTS

This research was supported by the Korea Research Foundation (KRF), NSF, and NASA.

[1] P.L. Altick, Phys. Rev. **169**, 21 (1968).
[2] G. Mehlman-Balloffet and J.M. Esteva, Astrophys. J. **157**, 945 (1969).
[3] J.M. Esteva, G. Mehlman-Balloffet, and J. Romand, J. Quant. Spectrosc. Radiat. Transf. **12**, 1291 (1972).
[4] J. Dubau and J. Wells, J. Phys. B **6**, L31 (1973).
[5] C.H. Greene, Phys. Rev. A **23**, 661 (1981).
[6] C.D. Lin, J. Phys. B **16**, 723 (1983).
[7] P.F. O'Mahony and C.H. Greene, Phys. Rev. A **31**, 250 (1985).
[8] V. Radojevic and W.R. Johnson, Phys. Rev. A **31**, 2991 (1985).
[9] R. Moccia and P. Spizzo, J. Phys. B **18**, 3537 (1985).
[10] J.A. Tully, M.J. Seaton, and K.A. Berrington, J. Phys. B **23**, 3811 (1990).
[11] H.-C. Chi, K.-N. Huang, and K.T. Cheng, Phys. Rev. A **43**, 2542 (1991).
[12] T.N. Chang and X. Tang, Phys. Rev. A **46**, R2209 (1992); **46**, R2209 (1992); T.N Chang and L. Zhu, *ibid.* **48**, R1725 (1993).
[13] B. Zhou and C.D. Lin, Phys. Rev. A **51**, 1286 (1995).
[14] D.-S. Kim, S.S. Tayal, H.-L. Zhou, and S.T. Manson, Phys. Rev. A **61**, 062701 (2000).
[15] M.J. Seaton, J. Phys. B **20**, 6363 (1987).
[16] F. Robicheaux and C.H. Greene, Phys. Rev. A **46**, 3821 (1992).
[17] F. O'Mahony and C.H. Greene, Phys. Rev. A **31**, 250 (1985).
[18] C.H. Greene, Phys. Rev. A **32**, 1880 (1985).
[19] D.-S. Kim and S.S. Tayal, J. Phys. B **33**, 3235 (2000).
[20] http://physics.nist.gov/cgi-bin/AtData/main_asd
[21] C.H. Greene and Ch. Jungen, Adv. At. Mol. Phys. **21**, 51 (1985).
[22] M. Aymar, C.H. Greene, and E. Luc-Koenig, Rev. Mod. Phys. **68**, 1015 (1996).
[23] C. E. Moore, *Atomic Energy Levels*, Natl. Bur. Stand. (U.S) Circ. No. 467 (U.S. GPO, Washington, DC, 1949), Vol. I.
[24] B.C. Fawcett, At. Data Nucl. Data Tables **16**, 135 (1975).
[25] R. Beigang, D. Schimidt, and P.J. West, J. Phys. (Paris), Colloq. **44**, C7-229 (1983).